JOURNAL OF GEOPHYSICAL RESEARCH, VOL. 95, NO. A10, PAGES 17,217–17,231, OCTOBER 1, 1990

Subionospheric VLF "Imaging" of Lightning-Induced Electron Precipitation From the Magnetosphere

UMRAN S. INAN, FRANK A. KNIFSEND, AND JANE OH

STAR Laboratory, Stanford University, Stanford, California

High-resolution measurements of subionospheric VLF signals at multiple sites are used as a new tool to assess the spatial distribution and occurrence of ionospheric disturbances associated with lightning-induced electron precipitation. Simultaneous observations in California, Saskatchewan, and Quebec of VLF signals from multiple sources allow the monitoring of event activity over a coarse grid covering the continental United States. Association of the observed VLF signal perturbations with lightning is often made on the basis of time correlation with prominent radio atmospherics. Simultaneous observations of individual events on subionospheric paths that "cross" one another are used to locate the disturbed ionospheric region(s). Absence of perturbations on nearby paths permits assessment of the spatial extent of the region with a varying degree of accuracy, depending on the distribution of signal paths. In one case distinctly different onset delays (with respect to causative discharges) consistent with predictions of whistler-particle scattering theory were found, and were interpreted as being due to two separate regions separated in L value by ~ 0.4 L being excited in individual events. Occurrence statistics over the course of October 1987 exhibit generally higher levels of activity at the lower-latitude end of the $2 < L < 4$ range, although it is difficult to separately assess the role of the source lightning distribution. Occurrence statistics of simultaneous events on crossing paths are consistent with the spatial extent of the disturbed ionospheric regions being less than a few hundred kilometers. The occurrence statistics also suggest that scattering from disturbances located at distances of > 100 km off the great circle paths is not significant.

1. INTRODUCTION

Characteristic changes in amplitude and/or phase of subionospheric VLF signals, commonly known as "Trimpi" effects, are believed to be signatures of ionospheric disturbances due to precipitating energetic electron bursts induced by whistler waves originating in lightning discharges. Important progress has been made on the interpretation of these whistler-associated amplitude [e.g., *Carpenter and LaBelle*, 1982] and phase changes [*Lohrey and Kaiser*, 1979; *Inan and Carpenter*, 1987], quantitative interpretation of events in terms of precipitated electron fluxes and energies [*Tolstoy et al.*, 1986; *Inan et al.*, 1985; *Inan and Carpenter*, 1987; *Inan et al.*, 1988*a*], association of events with whistlers [*Inan and Carpenter*, 1986] or with lightning discharges [*Inan et al.*, 1988*b*], and interpretation of events in terms of three-dimensional models of VLF propagation in the Earth-ionosphere waveguide [*Dowden and Adams*, 1988, 1989; *Poulsen et al.*, 1990].

Together with satellite- [*Voss et al.*, 1984] and rocket-based observations [*Rycroft*, 1973; *Goldberg et al.*, 1986], these new results have demonstrated the potential importance of lightning discharges in the upward/downward coupling of the atmospheric regions and in the loss of radiation belt particles. There is strong evidence that such coupling occurs in individual events, that individual whistler waves remove particles from the radiation belts, and that Trimpi events as observed on individual VLF paths occur quite frequently. However, full assessment of the importance of the phenomena on a global scale requires the knowledge of the geographic distribution of event occurrence and the spatial size and distribution of disturbed ionospheric region(s).

In this paper, we use subionospheric VLF observations at multiple locations in the northern hemisphere to (1) determine the occurrence patterns of Trimpi events over the continental United States, and (2) localize affected ionospheric regions by means of simultaneous perturbations on crossing subionospheric VLF paths. Our preliminary results illustrate the potential use of ground-based VLF remote sensing in "imaging" Trimpi events.

Paper number 90JA01278.
0148-0227/90/90JA-01278$05.00

2. DESCRIPTION OF EXPERIMENT

The VLF data described here were acquired at Lake Mistissini, Quebec (50°N, 74°W, $L \simeq 4.9$), Saskatoon, Saskatchewan (51°N, 107°W, $L \simeq 4.0$), and Stanford, California (37°N, 122°W, $L \simeq 1.8$). The geometry of the observations and VLF/LF signal paths is shown in Figure 1. Data are acquired during nighttime, typically for 12-14 hour periods. Amplitudes of VLF/LF signals is measured using narrowband receivers with a bandwidth of ~ 300 Hz. The detected envelopes of the receiver outputs are sampled at a basic rate of 100 Hz. Averaging is performed on site to obtain the lower sampling rates (typically 20 or 50 Hz) at which the data are recorded on digital tape. Summary plots of the data from all channels are printed out at the end of each day, displaying data with a 1-s time resolution and a time scale of 0.2 cm/min. These data were used for initial event identification as well as for the occurrence statistics reported in section 5.

Timing information is acquired from the GOES satellite with 1.5-ms accuracy at all three stations. The main sources of the background noise in narrowband channel outputs are radio atmospherics due to distant and nearby lightning. The background noise level varies as a function of location and frequency; however, the transmitter signal intensities are usually strong so that the signal-to-noise ratio in the receiver channels is generally ~10-15 dB. The threshold of detection of Trimpi events is not necessarily determined by the magnitude of the noise fluctuations; the noise is stationary in time, and transient amplitude changes with the characteristic Trimpi signature can be detected even if their magnitudes are smaller than the noise fluctuations. In general, Trimpi events involving amplitude changes of $> 5\%$ were unambiguously identifiable. The narrowband receivers employ fast responding (<1 μs) clipper circuits to limit the interference from radio atmospherics. Thus, the measured spheric signatures cannot

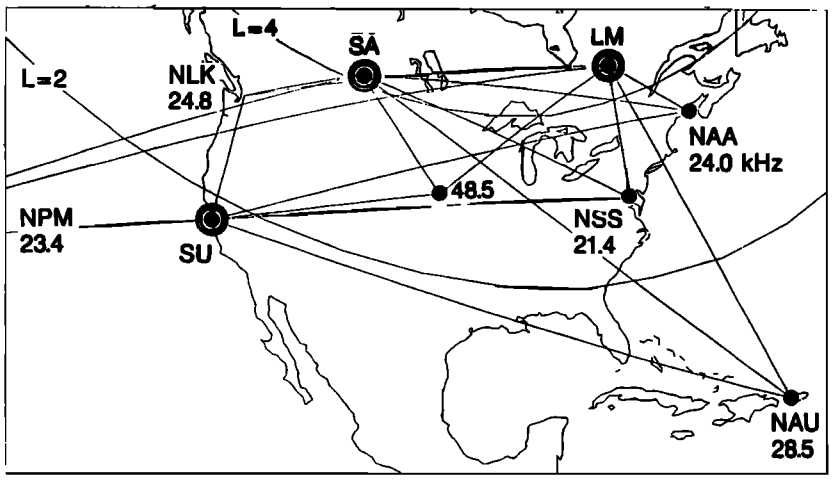

Fig. 1. Map showing the subionospheric VLF/LF paths observed at Stanford (SU), California, at Lake Mistissini (LM), Quebec, and at Saskatoon (SA), Saskatchewan. The NPM transmitter is located in Lualualei, Hawaii. The loci of the footprint of the $L = 2$ and $L = 4$ field lines at 100 km are also shown.

be used to extract calibrated amplitude and are only utilized to identify the times of occurrence of strong radio atmospherics.

The data shown in this paper were recorded in the month of October 1987. This month was chosen in view of the relatively high level of event activity and also because of data availability from all three stations. Selected individual events are discussed in section 4, and occurrence statistics from all three sites are presented in section 5.

A list of the VLF transmitters and their operating frequencies is given in Table 1. In the following discussion, we identify the data displayed with reference to the VLF/LF paths shown in Figure 1. For example, when the amplitude of the NSS transmitter signal as observed at Stanford (SU) is concerned, we denote this as the NSS-SU path.

TABLE 1. VLF/LF Transmitters

Call Sign	Transmitter	Frequency, kHz	Latitude, °N	Longitude, °W
NSS	USN Maryland	21.4	39	76
NPM	USN Hawaii	23.4	21	158
NAU	USN Puerto Rico	28.5	18	67
NAA	USN Maine	24.0	45	67
NLK	USN Washington	24.8	48	122
	USAF Nebraska	48.5	42	98

3. Subionospheric VLF "Imaging"

High-resolution measurement of amplitude and/or phase of subionospheric VLF signals has recently emerged as a sensitive new tool for detection of ionospheric disturbances associated with lightning discharges. Compared to other techniques for remotely sensing the ionosphere (such as riometers, photometers, etc.), this technique is not yet fully developed in terms of quantitative interpretation of the intensity, location and spatial distribution of the detected ionospheric disturbances. In principle, there is an ambiguity in terms of the location since observed perturbations may be due to ionospheric disturbances anywhere along or in the close vicinity of the great circle propagation path. On the other hand, the detection of ionospheric disturbances on such long VLF paths allows for observations of events occurring over widely distributed regions, as compared to other techniques that measure effects of disturbances in fairly limited fields of view. In this connection, we also note that the subionospheric VLF measurement is the only ground-based technique with which ionospheric effects of lightning-induced electron precipitation have been observed inside the plasmasphere [*Carpenter and Inan*, 1987]. This result could partially be due to the ability to monitor events over large regions and partially due to the fact that the VLF technique may be particularly sensitive to secondary ionization generated at nighttime D region altitudes by precipitating > 40-keV electrons. As improved models of subionospheric propagation in the presence of localized disturbances become available [*Dowden and Adams*, 1988, 1989; *Poulsen et al.*, 1990], we can expect to quantitatively evaluate the possible location of the disturbed regions along or near the great circle paths in individual cases. In the meantime, the simple occurrence or not of VLF perturbations on a distributed network of paths (Figure 1) may well allow us to locate the regions involved in some cases and to possibly place some limits on their spatial extent.

While this type of "imaging" is the topic of the present paper, the reader should be cautioned ahead of time concerning the underlying assumptions. It is important to note, for example, the relative sensitivity of different subionospheric paths to a given ionospheric disturbance. Each path has a different distribution of waveguide modes whose sum constitutes the detected signal at the receiver. Paths for which the receiver location may be near a minimum are expected to be more sensitive, since small changes in components of the sum could lead to relatively large changes in the resultant [*Tolstoy et al.*, 1982; *Wolf*, 1990]. In view of this, absence of characteristic perturbations on a certain signal does not necessarily imply absence of ionospheric disturbances directly on or near the signal path. By the same token, an ionospheric disturbance that perturbs one signal path may not necessarily produce a detectable perturbation on another path nearby. Furthermore, the size of the VLF signal perturbation (amplitude and/or phase change) is not necessarily a simple function of the transverse or vertical extent or the magnitude (i.e., amount of excess secondary ionization) of the ionospheric disturbance and is expected to be dependent on the waveguide mode structure.

Given these limitations, we nevertheless proceed in the rest of the paper by assuming that the presence or absence of perturbations on a signal is a good indication of the existence or lack of

ionospheric disturbances along or near the path. Our analysis in this paper is aimed at determining what conclusions can be deduced subject to this assumption. The validity of this assumption will need to be addressed as improved models of subionospheric VLF propagation are developed. In this connection, it is useful to note that three-dimensional modeling of subionospheric propagation for cases involving a single dominant waveguide mode shows that effects of disturbances located off from the great circle path decrease rapidly with distance from the path, becoming negligible for disturbances located at transverse distances of > 100 km [*Poulsen et al.*, 1990].

In the rest of this paper, we explore the potential of this subionospheric VLF technique as a means of "imaging" lightning-induced electron precipitation events. We first illustrate selected examples of events occurring on "crossing" subionospheric paths suggesting that the disturbed ionospheric regions are located near the crossing points. Subject to the caveats discussed above, we use the lack of events on adjacent paths as a way to place limits on the transverse extent of the disturbed region(s). We then present occurrence statistics of Trimpi events on the VLF paths shown in Figure 1 in order to assess the distribution of disturbed ionospheric regions on a continental scale. Statistics of simultaneous events on multiple paths are presented in section 6 as a means of assessing the transverse size of ionospheric region(s) disturbed in individual events, recognizing that larger regions would overlap more paths and lead to a higher likelihood of simultaneous events.

4. Examples of Trimpi Events on Crossing VLF Paths

In this section, we present examples from three cases in which simultaneous Trimpi events were observed at Stanford and at Saskatoon on subionospheric paths that "cross" one another. Our purpose here is to illustrate that information on the location and size of disturbed ionospheric regions can be extracted in individual cases, subject to the basic assumptions and reservations discussed in the previous section.

Case 1: October 10, 1987

The top panel in Figure 2 shows a 30-min sequence of events observed on the 48.5-SA path on October 10, 1987. The events are clearly identifiable on the basis of their known characteristic signature, involving rapid (< 1 s) onsets followed by relatively slow (10-100 s) recoveries [*Inan and Carpenter*, 1987]. The lower panel in Figure 2 shows a simultaneous record of the NAA-SU signal, which shows a perturbation at the same time (within the 1.2-s resolution of this record) with the first and largest event on the 48.5-SA path occurring at 1132:00 UT. (The drop in the NAA signal at ~1134:00 UT was also recorded at SA and is attributed to interruption of the transmission at the source.) We note that the second largest 48.5-SA event occurring at ~1151:30 UT is also registered on the NAA-SU signal.

The simultaneity of the two events at higher resolution is illustrated in Figure 3. The left hand panels show a 200-s data record showing the 48.5-SA and NAA-SU paths, as well as the amplitude in the 48.5±0.15 kHz band received at Stanford (48.5-SU signal). While no Trimpi events are observed on the 48.5-SU path, this channel is useful as a means of identifying causative radio atmospherics superimposed on the transmitter signal. In the case shown, a clear isolated spike in the 48.5-SU channel is apparently coincident with the Trimpi events on the upper two panels. The panels on the right show a further expanded version of the data. In this 10-s record displaying the raw data with no averaging, the radio atmospheric is clearly visible in the 48.5-SU, 48.5-SA, and NAA-SU channels. The Trimpi event in the 48.5-SA channel displays all the classical features, including a ~ 1.2-s onset delay (between causative atmospheric and event onset), as well as an ~ 0.5-s onset duration (risetime) which may be indicative of the duration of the precipitation burst [*Inan and Carpenter*, 1986]. The simultaneous Trimpi event in the NAA-SU channel is less well defined, but basically has the same temporal characteristics as the 48.5-SA event.

We note here that the association of radio atmospherics with Trimpi event onsets is generally established on the basis of repeatability of the signatures. Similar spheric signatures (sharp

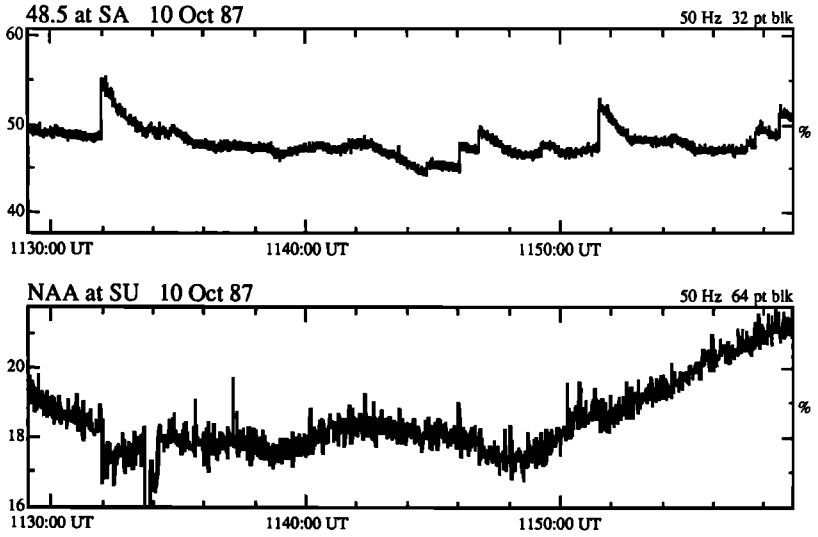

Fig. 2. The top panel shows a 30-min sequence of events on the 48.5-SA path. The drop in the NAA-SU signal ~1134 UT is due to transmitter interruption (recorded also at SA). The vertical scale is linear, showing signal amplitude (A) in arbitrary units, with $A = 0$ representing absence of signal. The numbers shown on the ordinate correspond to the percentage of full scale. Thus, the first event at 1132 UT (top panel) represents an amplitude change of 5 units on top of an ambient level of 50 units, i.e., a 10% event. The data in the top and bottom panels represent detected amplitude time averaged over 0.64 s and 1.28 s, respectively.

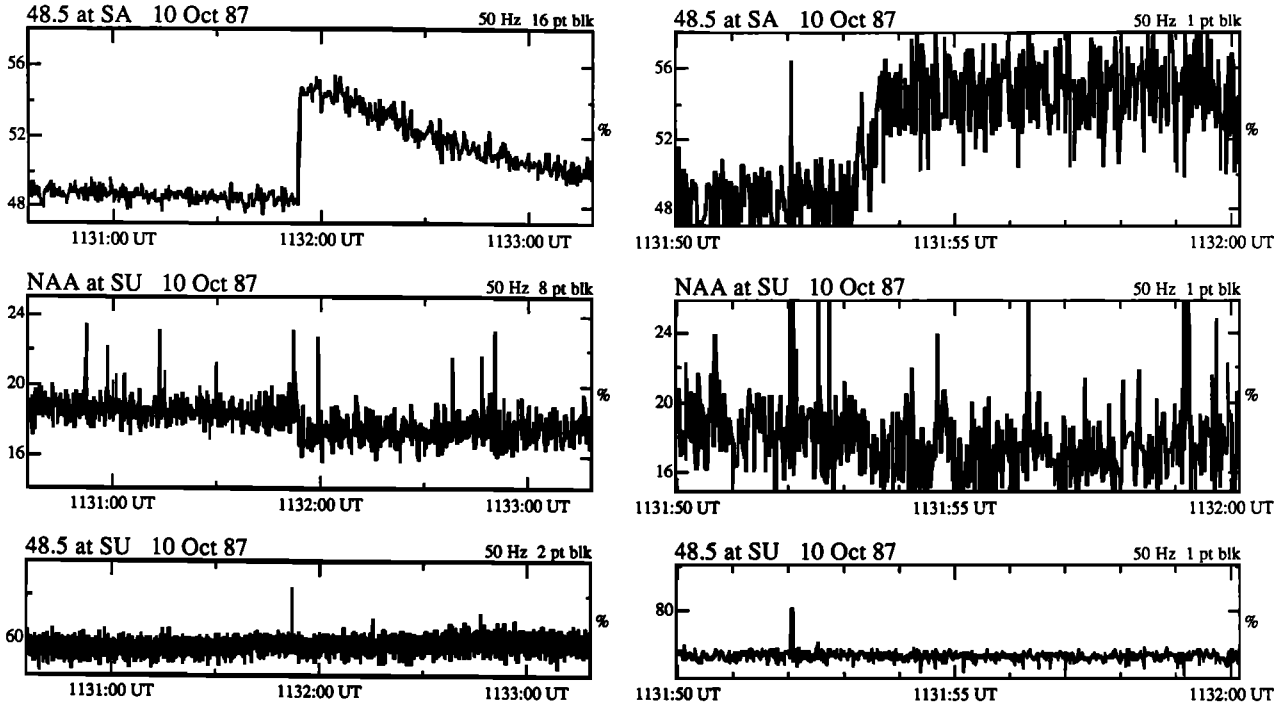

Fig. 3. High-resolution displays of the largest event shown in Figure 2. The format of the data displays is similar to that of Figure 2. The panels on the right show the 20-ms samples without averaging, while the panels on the left are time averaged over 0.32 s (top), 0.16 s (middle) and 0.04 s (lower). The causative spheric and the negative perturbation simultaneous with the well-defined event at 48.5-SA are both apparent on the NAA-SU signal. The absence of other spherics of comparable amplitude on the 48.5-SU signal make the causative spheric easily identifiable. The panels on the right show the same event at higher resolution. The causative spheric precedes the event by ~1.2 s.

peaks preceding the event onsets by ~1.2 s) were observed in at least one or more of the receiver channels for all the events observed on the 48.5-SA signal that are displayed in the upper panel of Figure 2.

The temporal characteristics of the event as illustrated in Figure 3 can be compared with theoretical estimates provided by *Chang and Inan* [1985]. Note that the crossing of the NAA-SU and 48.5-SA paths is at 43.9°N, 99.6°W (L = 2.92). For L = 3.0, cold plasma density at the equator of 600 cm^{-3}, and for a typical whistler, the computed arrival time for the peak precipitation is 0.9 s, and the duration of the precipitation burst is 0.4 s [*Chang and Inan*, 1985]. Considering the uncertainty in the plasma density, and the fact that the density at L = 3.0 is generally closer to 1000 cm^{-3} [*Park et al.*, 1978], the measured onset delay of ~ 1.2 s and onset duration of ~ 0.5 s are consistent with the theoretical estimates.

The simultaneity of the events observed on the 48.5-SA and NAA-SU paths is consistent with an ionospheric disturbance in the vicinity of the crossing point of these two paths. Equally important in this consideration is the absence of events on the other VLF paths that were observed on SU and SA on this day (no data were available from LM for October 10, 1987). Subject to the assumptions as discussed in section 3, it would appear that the disturbed region was probably not directly above the 48.5-kHz transmitter since the 48.5-SU path did not register any perturbation (Figure 3). Also, the eastern edge of the disturbed region probably did not overlap the NAU-SA path, since this path did not register any events. The southernmost extent of the region could be bounded by the lack of events on the 48.5-SU and NSS-SU paths. With the path configurations shown in Figure 1, we do not have enough information to restrict the disturbed region in terms of its western and northern extents. It is also interesting that only the largest two events observed on the 48.5-SA path were detected on the NAA-SU path; such a circumstance is consistent with a perturbed region lying near the middle of the 48.5-SA path and having a radius (if indeed circular in shape) proportional to the size of the VLF amplitude change. In such a case, the southernmost extent of the disturbance would have overlapped the NAA-SU path in the case of the largest events.

Case 2: October 15, 1987

Figure 4 shows a sequence of events observed at both Saskatoon and Stanford on October 15, 1987. Data were also available on this day from Lake Mistissini. The format of Figure 4 is similar to that of Figure 2. We note that several events are observed on the 48.5-SU path, some of which are common to the NSS-SU and NAA-SU paths. The time period shown represents a 30-min segment of the period 0300-0500 UT during which ~20 events (amplitude changes > 5%) were observed on the 48.5-SU signal. During this same period, the 48.5-SA signal exhibited fluctuations, typical of relatively disturbed conditions ($\sum Kp >$ 29 for October 13, 14, and 15, 1987) at relatively higher latitudes outside the plasmapause (Saskatoon is at $L \simeq 4$).

Other paths observed at Saskatoon, such as NPM-SA, exhibited a high degree of variability, sometimes (for example during the 0315-0325 UT period) with very similar fine structure to that seen on the 48.5-SA path, being consistent with a disturbed ionosphere above the receiver site. In addition, many of the paths observed at Lake Mistissini ($L \simeq 4.9$), including the 48.5-LM signal, were similarly perturbed during this same period. Selected signals observed at LM and SA are shown in Figure 5 to illustrate the difference between low-latitude and mid- to high-latitude paths in comparison with the lower two panels of Figure 4. Such

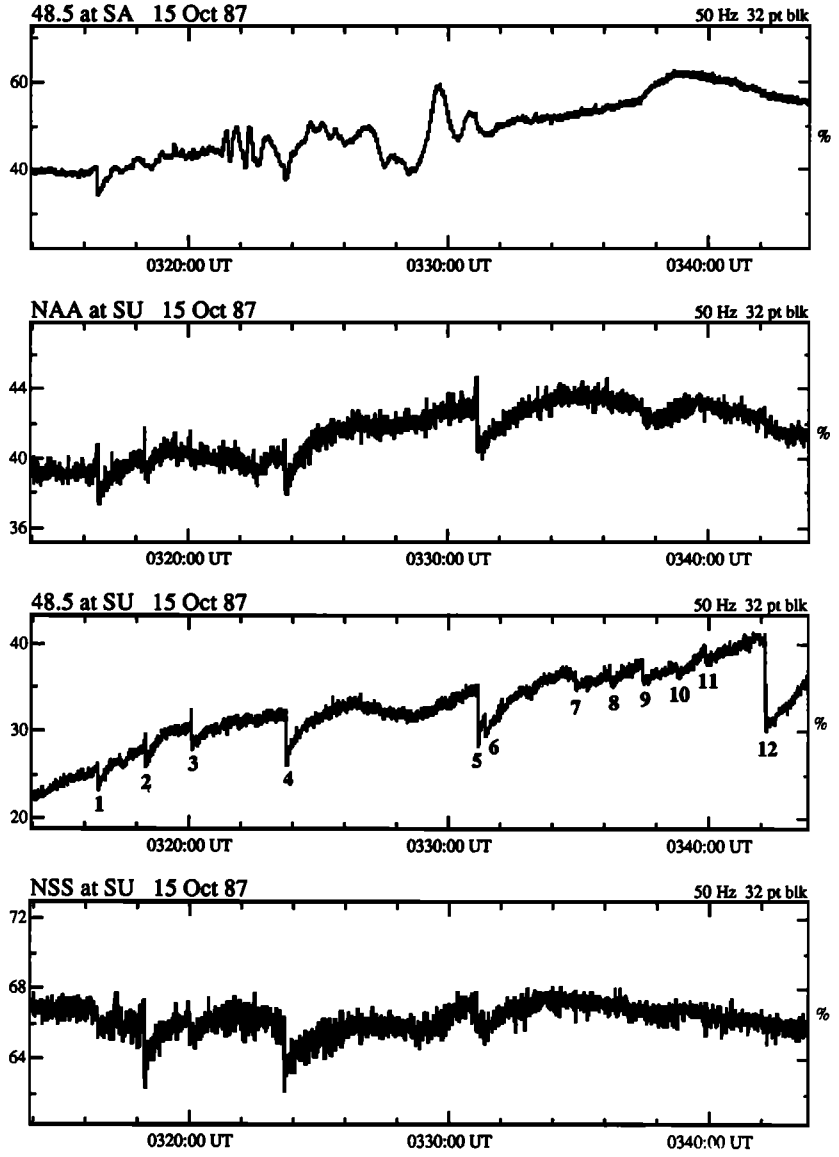

Fig. 4. Thirty-minute sequence of events observed at both Saskatoon and Stanford. Events on 48.5-SU are numbered in order of occurrence. The format is similar to that of Figure 2. The data shown were time averaged over 0.64 s.

irregular variations on the signal amplitudes are often observed at LM and SA and may themselves be very useful in the investigation of subauroral background drizzle precipitation effects. In this paper, we concentrate on Trimpi events, easily identifiable on the basis of their characteristic signature, even in the midst of other fluctuations such as those shown in Figure 5 (also see Figure 8).

We observe from Figure 4 that the first Trimpi event (marked by 1) clearly seen on the NAA-SU, 48.5-SU, and NSS-SU paths is accompanied by a distinct event signature on the 48.5-SA path. The subsequent events on the Stanford paths, i.e., those marked 2, 3, 4, and 5, are much harder to identify on the 48.5-SA path; however, careful examination shows the presence of a relatively rapid onset (decreases in amplitude for both events 4 and 5 and amplitude increase for event 2) on the record in Figure 4 and also, more clearly, on higher-resolution records that were separately examined.

The event signatures at higher resolution are shown in Figure 6 for two of the events (1 and 4) from Figure 4 and reveal a clear difference in the temporal signature of the 48.5-SU and NSS-SU signals shown in the lower two panels and the NAA-SU and 48.5-SA signals displayed in the upper panels. The sharp peak apparent in all channels indicates a common causative radio atmospheric; however, the time delay from the spheric to the event onset is ~0.65 s for NSS-SU and 48.5-SU, while being ~1.1 s for the NAA-SU and 48.5-SA events. The same circumstance is common to both of the events shown and was also found to be the case for the other well-defined events observed during the 0300-0500 UT period on this day.

The result illustrated in Figure 6 is consistent with two separate ionospheric regions being disturbed by the same lightning discharge. Considering the map of signal paths given in Figure 1, one of these regions could be in the vicinity of the crossing point of the 48.5-SA and NAA-SU paths, while the second one could be located to the west of the 48.5-kHz transmitter, on or near the 48.5-SU and NSS-SU paths. We note that the disturbed region is not likely to be above the 48.5-kHz transmitter, since the 48.5-LM path was not perturbed and also since the onset delays for the 48.5-SA and the 48.5-SU paths are clearly different.

An expanded view of the region in the vicinity of the 48.5-kHz transmitter together with all the propagation paths from Figure 1

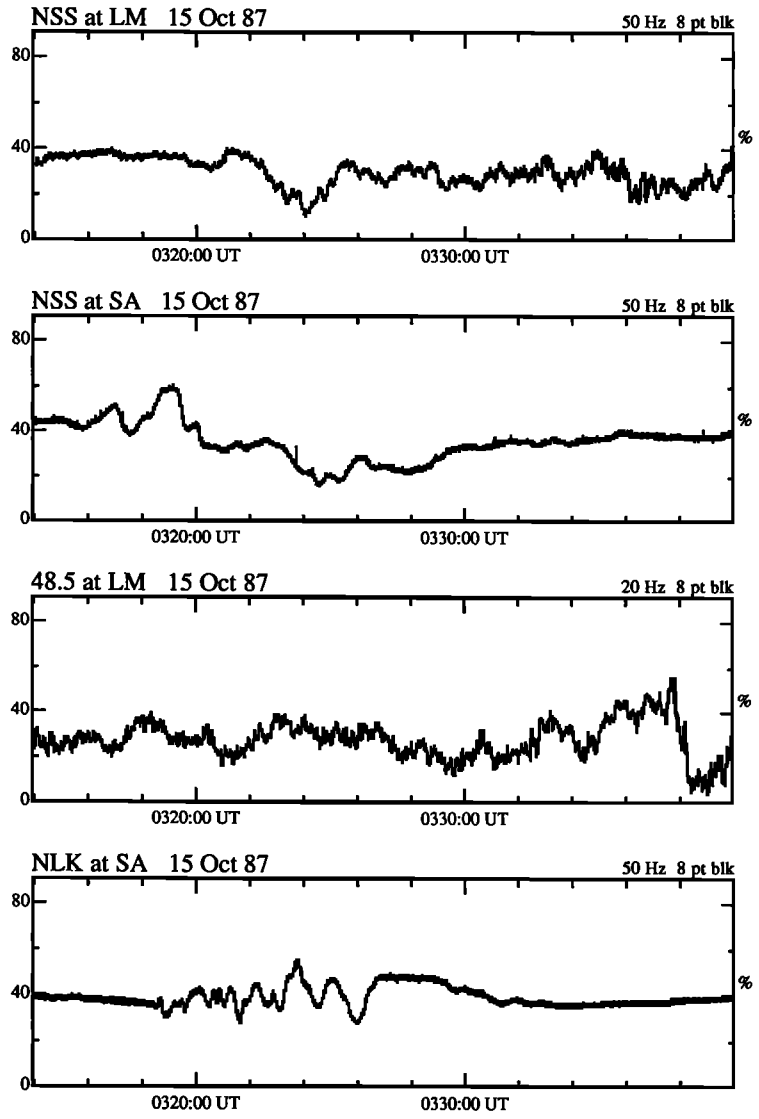

Fig. 5. Selected paths observed at LM and SA to be compared with 48.5-SU and NSS-SU shown in Figure 4. The format is similar to that of Figure 4. The data shown were time averaged over 0.16 s, except for 48.5-LM, which is averaged over 0.40 s.

is shown in Figure 7. Two possible disturbed ionospheric regions are identified as I and II on Figure 7. The first (I) of the two separate regions could be at the crossing of the NAA-SU and 48.5-SA paths (43.9°N, 99.6°W, L = 2.9). While the location of the second region (II) cannot be specified as easily, assuming that it is at the same longitude (99.6°W) as region I and centered between the NSS-SU and 48.5-SU paths (as shown in Figure 7) gives ~41°N or $L \simeq 2.5$. If this second region were further west, the L value would be somewhat lower. In any case, it appears that the difference in L value between the two separate regions could be as much as 0.4-0.5L. The ~ 0.45-s time difference between the onset delays for these two regions could be due to a combination of the higher travel time for the whistlers and the lower energy of the resonant electrons that would be expected at the higher L shell. A test particle model comparison of temporal signatures of electron precipitation bursts as a function of L shell has been done by *Chang and Inan* [1985], for a specific cold plasma density profile with a density at L = 2.5 of 1000 cm^{-3}. Results presented in Figure 8 of *Chang and Inan* [1985] for the arrival time of the peak of the precipitation burst give 0.5 s for L = 2.5 versus 0.9 s for L = 3. Considering the uncertainty in the plasma density, and the fact that the density at L = 2.5 is generally closer to 2000 cm^{-3} [*Park et al.*, 1978], the onset times of ~ 0.65 s and ~ 1.1 s are consistent with the notion of there being two separate disturbed ionospheric regions at $L \simeq 2.5$ and $L \simeq 2.9$, respectively.

Due to the absence of whistler data from the southern hemisphere, we do not have enough information to determine whether the ionospheric disturbances are due to precipitation induced by ducted or nonducted whistlers. However, the apparently separate nature of the two disturbed regions, the fact that the onset delays for both are consistent with those expected on the basis of theoretical estimates that assume ducted propagation [*Chang and Inan*, 1985], and the more general result (discussed below) that simultaneous perturbations on crossing paths occur rarely are all consistent with the disturbed ionospheric regions being located at the ends of magnetospheric whistler ducts.

The Stanford data for the October 15, 1987 case were also investigated as part of a separate study of the spatial relationship between lightning discharges (as detected by ground-based networks) and perturbed VLF/LF propagation paths (W. Y. Yip et al., On the spatial relationship between lightning discharges and

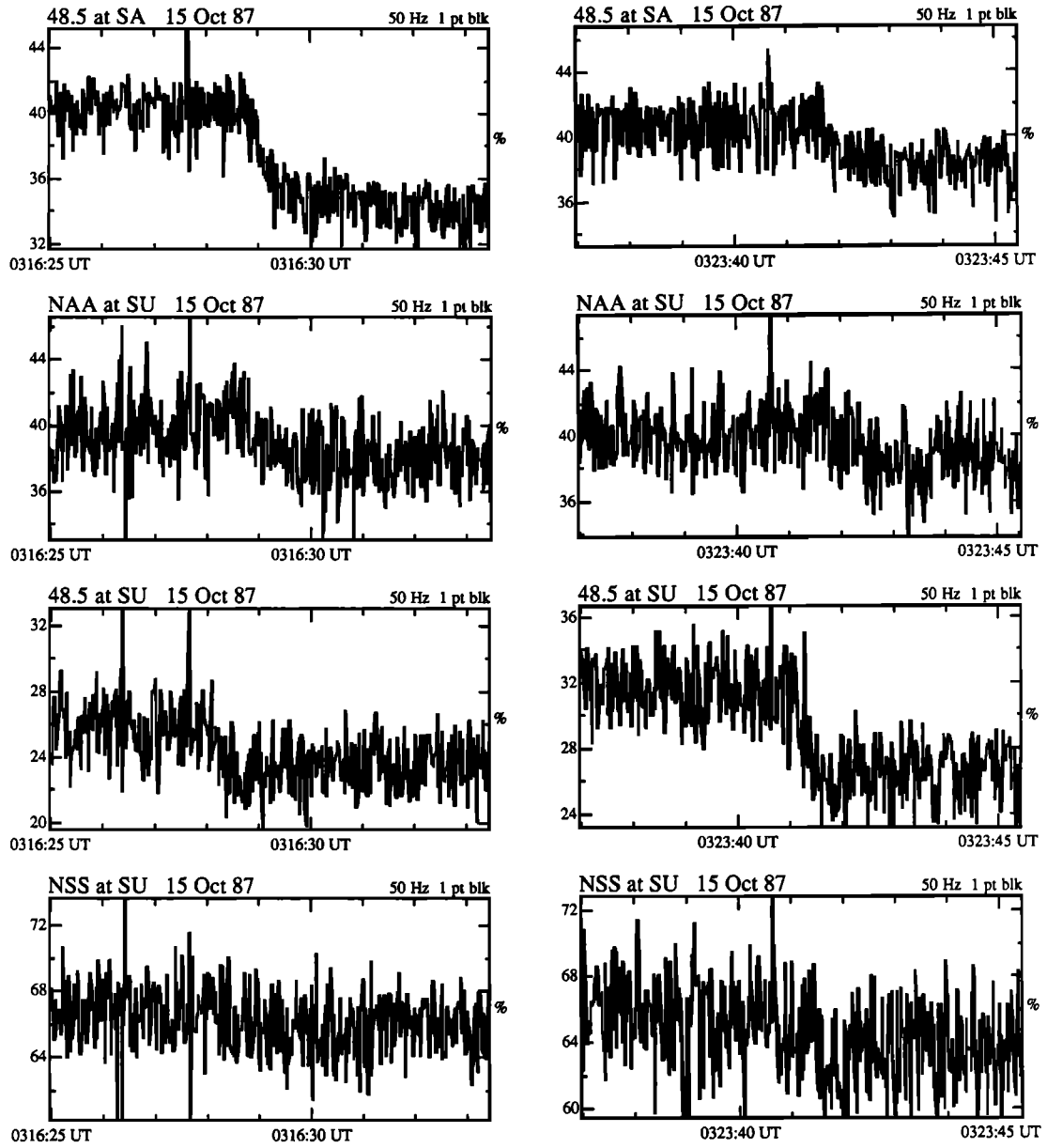

Fig. 6. High-resolution displays for events 1 (left) and 4 (right) from Figure 4. The format is similar to that of Figure 3. In each panel the 20-ms data samples are shown without averaging. The causative spherics are most clearly seen in the 48.5-SA channel although they are also visible in the other panels. Similar causative spherics were found for other events observed during the 0300-0500 UT period on this day.

propagation paths of the perturbed subionospheric VLF/LF signals, submitted to *Journal of Geophysical Research*, 1990, hereinafter Yip et al., submitted manuscript, 1990). The only active thunderstorm over the continental United States during the period of 0300-0500 UT on this day was located in New Mexico, with the nearest detected cloud-to-ground flashes being > 500 km due south of the NSS-SU path. In four separate days including October 15, 1987, it was found that lightning similarly located was associated with Trimpi events on the 48.5-SU path, while the NAU-SU path, on which the thunderstorm regions were centered, did not register any events. The conclusion was that, in those cases studied, the locations of the disturbed regions were more dominantly controlled by magnetospheric factors (such as L shell, availability of whistler ducts, and trapped particle distributions), rather than the source lightning distribution. Such a circumstance is consistent with our identification of two disturbed regions in this study, although noting from Figure 1 that the NAU-SU path crosses the $\sim 99°$W longitude at $L \simeq 1.8$, it is possible that additional disturbed regions (possibly other ducts) in the range $2 < L < 2.5$ may also have been excited.

It is difficult to extract more information on the spatial extent of the disturbed regions from the available data. However, some insight into the various possibilities may be gained by further examination of Figures 1 and 7, subject to the caveats discussed in section 3. If the two regions as discussed above are distinctly separate and equal in size, for example, then the southern extent of region I (or the northern extent of region II) would need to be < 150 km. The absence of perturbations on the NAU-SA path indicates that the eastern extent of region I is < 600 km, although a more stringent constraint is probably the fact that 48.5-LM is not perturbed, indicating that the two regions probably do not extend overhead the 48.5-kHz transmitter. The latter would

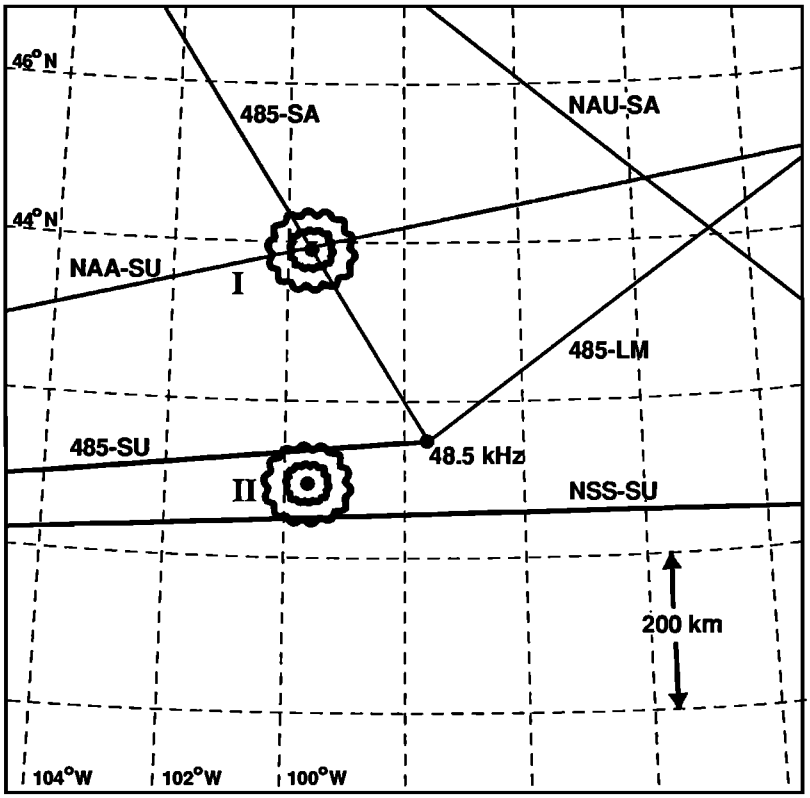

Fig. 7. An expanded view of the region around the 48.5-kHz transmitter located in Silver Creek, Nebraska, and the signal paths in this vicinity. Probable locations of the two separate disturbed regions (I and II) are shown, emphasizing that their boundaries and radial extent are unknown.

indicate that the eastern extent of region II is < 200 km and that the southeastern extent of region I is < 350 km.

Examination of the event sequence in Figure 4 suggests another possible clue to the spatial distribution of the perturbed regions. Considering the entire sequence of events on the 48.5-SU path as shown, we note that between 0314 and 0330 UT, events with larger-amplitude changes are generally associated with better-defined events on the NSS-SU and NAA-SU paths. This situation appears to change in the later part of the record, with events 7 through 12 not being accompanied by any detectable events on the NAA-SU and NSS-SU paths, is spite of the fact that event 12 is the largest event on the 48.5-SU signal for the period shown. In a separate study also mentioned above, this event was interpreted to be caused by a very intense and positive cloud-to-ground lightning flash that preceded the event onset by < 1 s. The causative lightning flash was detected by the lightning network in the midst of generally less intense and mostly negative flashes, some of which similarly preceded other Trimpi events such as 2, 8, 10 and 11 from Figure 4 (Yip et al., submitted manuscript, 1990). The high-resolution signature of event 12 shows no unusual features, with the onset delay and duration being very similar to the two 48.5-SU events shown in Figure 6.

In view of the path configurations shown in Figure 7, this result could come about if in this particular event (12) the disturbed ionospheric region was much closer to the 48.5-SU path and further away from the NSS-SU path. It is possible that the duct associated with region II drifted to higher latitudes, or that a separate (third) region much closer to the 48.5-SU path was selectively excited. Three-dimensional modeling of subionospheric VLF propagation shows that the effect of localized disturbances decreases rapidly with distance off the great circle path, being negligible when that distance is >100-200 km [*Poulsen et al.*, 1990]. Since the separation between the NSS-SU and the 48.5-SU paths at 99.6°W longitude is ~ 100 km, a disturbed region closer (by 50-100 km) to the 48.5-SU path than region II would be consistent with both the absence of an event on the NSS-SU path and the fact that the 48.5-kHz signal amplitude change for event 12 is larger than that for other events. However, if we pursue this hypothesis somewhat further, we would need to conclude that the north-south extent of the disturbed region must be < 100 km, in order for a change of 50-100 km in the location of the center of the region to make a difference in the response of the NSS-SU signal. We also note that in the next hour, during 0400-0500 UT, additional events were observed on the 48.5-SU path, some of which were accompanied by events with positive amplitude changes on the NSS-SU path, with the NAA-SA signal also being perturbed in association with an especially large 48.5-SU event. This variation in the character of the NSS-SU perturbations, from negative to zero to positive amplitude changes, is also consistent with northward motion of region II, or the excitation of a third region. If duct drift [*Carpenter and Seely*, 1976] was the cause of this northward motion, one would expect region I to move in a similar fashion, consistent with the absence of any associated signature on the NAA-SU signal for event 12.

Case 3: October 27, 1987

On October 27, 1987, there were five simultaneous Trimpi events seen on NAU-SA and NSS-SU during the 35-min period

of 0630-0705 UT. These two paths cross just south of the Great Lakes in the eastern United States, at $L \simeq 2.7$. Figure 8 shows the data from this period, while high time resolution displays of two of the events occurring at 0642:03 UT and 0704:06 UT are shown in Figure 9. We note from Figure 9 that these data exhibit a higher level of impulsive noise (corresponding to spheric activity) compared to those for cases 1 and 2. Data from a separate spheric channel at LM give an indication of intensity of prominent radio atmospherics in the range of 2-4 kHz. The causative spheric preceding the event onsets by < 1 s is seen on the lowest panels of Figure 9, and also in the NAU-SA and NSS-SA channels, for both of the events shown.

The delay from the causative spheric to the event onset is not as well defined as in cases 1 and 2 but is in the range of 0.6-0.8 s, consistent with that expected for this L shell range as discussed above [*Chang and Inan*, 1985]. There appears to be some difference in the duration of the onset between the NSS-SU and NAU-SA signatures for the event at 0704:06 UT, although this feature was not present in the other events during this period.

We note again, from Figure 8, the generally more perturbed nature of the signal paths, portions of which lie at higher latitudes. The NSS-SU signal exhibits slower variations than the NSS-SA and NSS-LM signals with the Trimpi events being the main source of variations that occur over time scales of a minute or so. The NSS-SA and NSS-LM signals are dominated by many more variations occurring over similar time scales, probably representing background drizzle precipitation effects occurring at the higher-latitude ends of these paths on subauroral field lines. However, we note that Trimpi events occurring in the midst of such other fluctuations are generally recognizable (as in the top panel

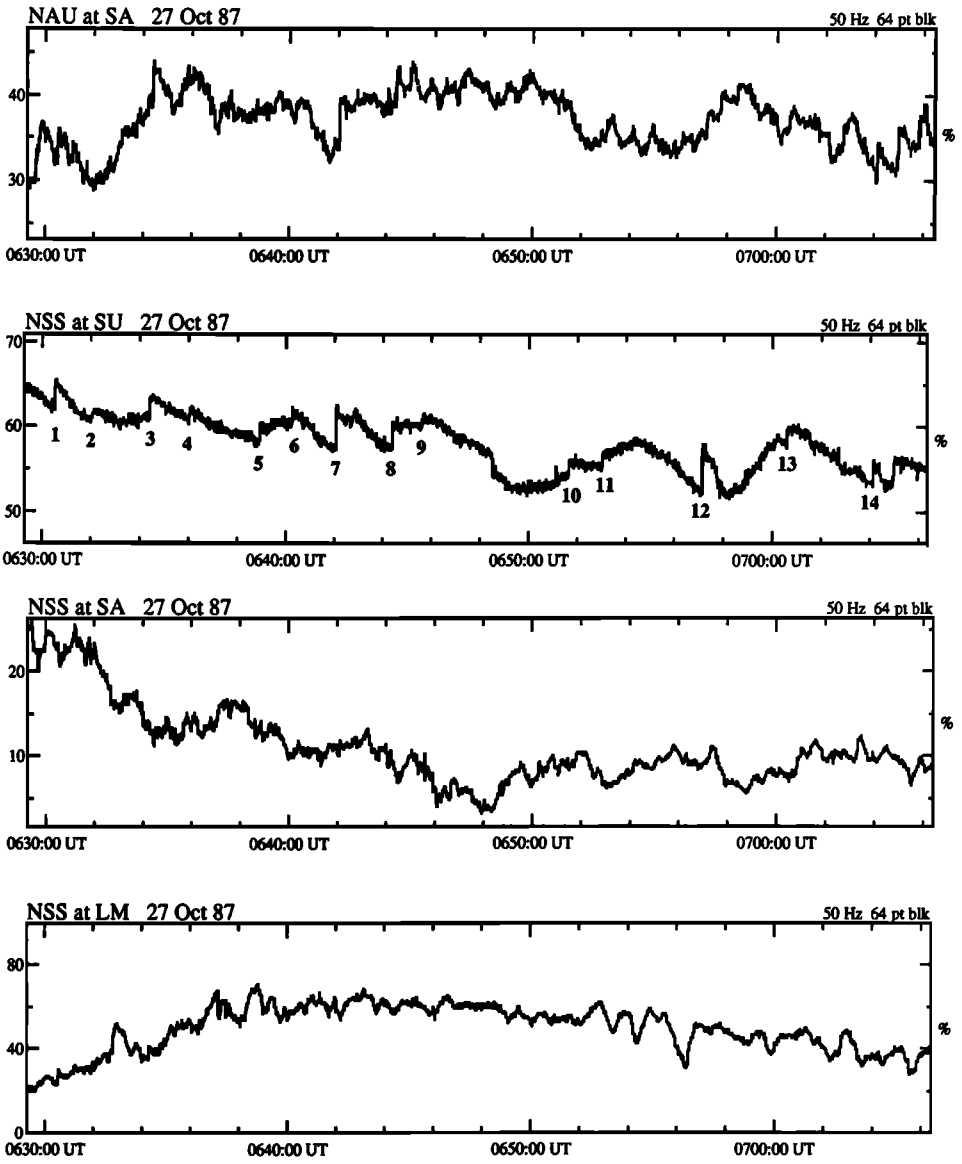

Fig. 8. Thirty-five-minute sequence of events observed on both NSS-SU and NAU-SA signals on October 27, 1987. Some of the better-defined events on the NSS-SU signal are enumerated. Events simultaneous with some of these are recognizable in the NAU-SA channel amidst signal fluctuations due to other ionospheric activity. No well-defined events on NSS-SA and NSS-LM are visible at this resolution. The format of the displays is similar to that of Figure 2, with the data shown being time averaged over 1.28 s.

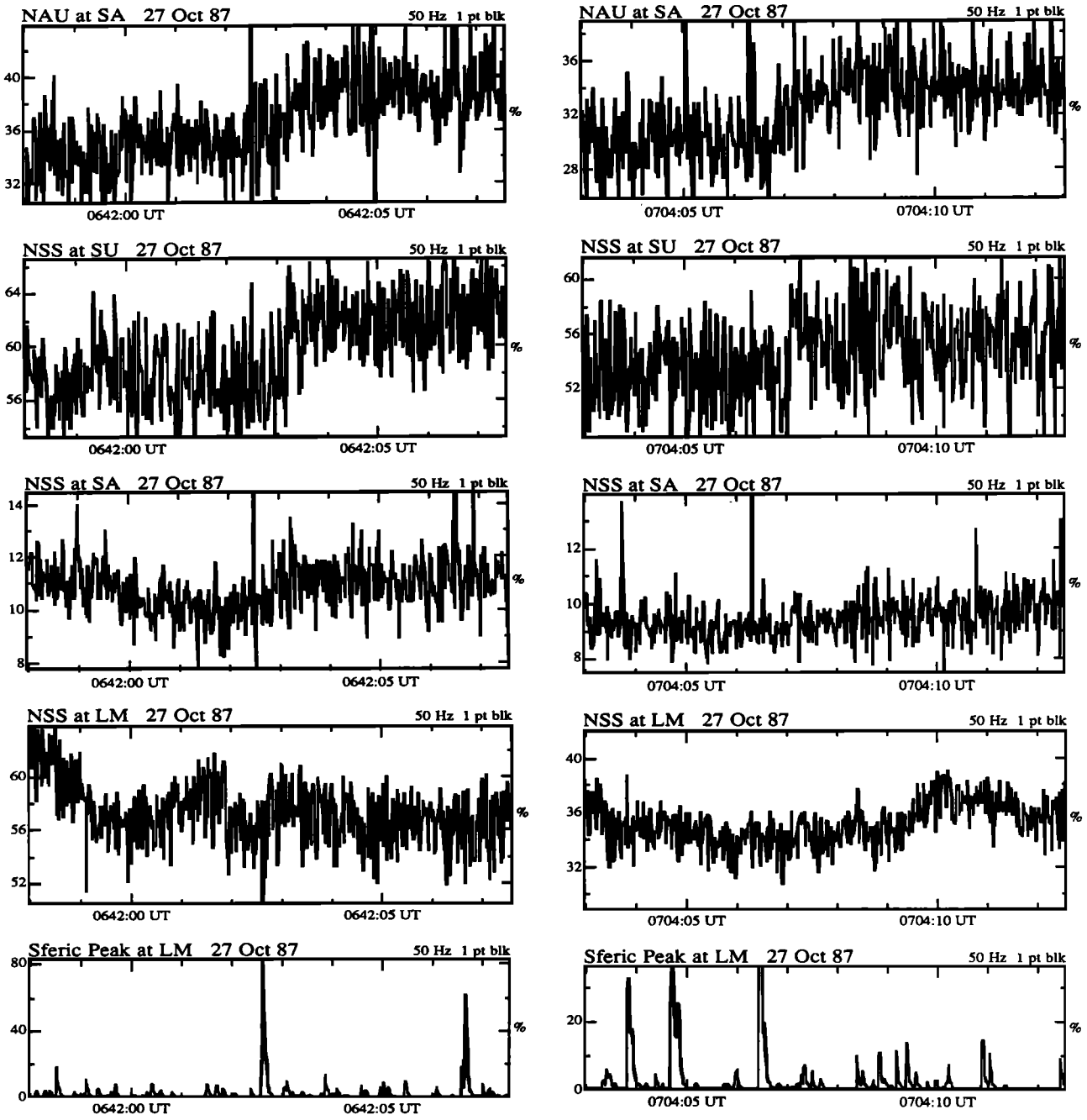

Fig. 9. High-resolution displays for two events 7 and 14 from the period shown in Figure 8. For the event at 0642:03 UT, a causative spheric is seen superimposed on all four signals shown as well as the spheric channel at Lake Mistissini shown in the bottom panel. The format is similar to that of Figure 3. The 20-ms data samples are shown without time averaging.

of Figure 8 and as was the case in the top panel of Figure 4) on the basis of their characteristically rapid (< 1 s) onset, followed by a slower (10-100 s) recovery.

We also note that unique determination of the causative spheric for simultaneous events is not always possible. In most of the cases we have examined, there is usually only a single spheric which both exhibits a significant amplitude and occurs within 1-2 s of the event onset so that it can positively be identified as the causative one. However, in some cases, and especially for those which occur closer to the east coast where the lightning activity is higher, there are multiple spherics preceding the event onset by 1-2 s. This was the case for the last event shown in Figure 8, occurring at 0704:59 UT.

The simultaneity of the events observed on the NAU-SA and NSS-SU paths during 0630-0705 UT is consistent with the disturbed ionospheric regions being located in the vicinity of the crossing point of these paths. The fact that there were no simultaneous events observed on the 48.5-LM and 48.5-SA paths to the west and the NSS-SA path to the east indicates that the disturbance lies within these boundaries. The extent of the southern boundary of the disturbed region is unknown due to lack of VLF paths south of the crossing point. The northeast boundary of the disturbance could lie very close to the NSS-SA path, as there is a slight perturbation appearing on that NSS-SA signal just after the causative spheric for the simultaneous events at 0642:03 UT (see Figure 9).

5. Occurrence Statistics

The examples shown in the previous sections illustrate the potential use of subionospheric VLF remote sensing as a means of "imaging" the ionospheric regions perturbed in association with lightning discharges. While such imaging on a small scale is important in determining the size and shape of perturbed region(s) in disturbed individual events, it is equally important to "image" the occurrence patterns of events on a continental scale. The latter is especially needed in order to be able to assess the importance of Trimpi effects on a global scale. In this section, we discuss the occurrence statistics of Trimpi events over the continental United States, as observed during October 1987 at Stanford, Saskatoon, and Lake Mistissini with the VLF/LF network of paths as shown in Figure 1.

Statistics of event occurrence were obtained by visual inspection of daily produced summary plots on which amplitudes of signals had been plotted after on site averaging (typically over 1 s). On these summary charts, the characteristic fast rise/slow decay signatures could be identified for amplitude changes of $\sim 5\%$ or greater. The results for each signal as observed at each of the receiving sites are shown in Figure 10 on a bar graph indicating the number of hours within which one or more events were observed on each day of October 1987. The bar graph format used in Figure 10 is similar to that used in previous presentations of occurrence data on Trimpi events [*Carpenter and Inan*, 1987; *Inan et al.*, 1988*c*].

A number of interesting features of the occurrence distribution can be noted from the data given in Figure 10 and are discussed below. We note that with the data in hand at the present time, it is not possible to determine whether the various differences in the activity on the paths are due to magnetospheric factors, relative sensitivity of different subionospheric paths, or source lightning distribution. The length of the path (or the area covered by the path) may also affect the statistics of event occurrence. However, the results shown are nevertheless a measure of event activity over the continent, and a brief discussion of the possible causes of the various differences is warranted.

At Lake Mistissini (LM), we find the NAU-LM, 48.5-LM, and NSS-LM paths to be more active than the NAA-LM and NLK-LM paths. In view of the path distribution shown in Figure 1, this result is consistent with generally higher levels of activity observed in the southern hemisphere in the region of $2 < L < 3$, with decreasing activity closer to $L = 4$ [*Carpenter and Inan*, 1987]. The same could be said about the NLK-SA path, which also has very few events. The NPM-LM path starts at lower latitudes but lies at higher latitudes ($L > 4$) over the eastern United States where lightning activity is prominent. We note that the NPM-SU and NPM-SA paths are also quite inactive, consistent with lack of lightning activity in the west coast regions. At Saskatoon, the NAU-SA path is by far the most active and is the only one that passes through the $2 < L < 2.5$ range. We also note that the NAU-LM path shows similar activity, while the NAU-SU path is somewhat less active than NAU-LM and NAU-SA, possibly due to its being at too low an L value. Another interesting pair to compare is the NSS-SU and NSS-SA paths. The former is substantially more active, due either to the L shell or the source lightning distribution. We also note that 48.5-SU is similarly active, presumably due to lightning activity in the southwestern United States (Yip et al., submitted manuscript, 1990). The difference in activity between the 48.5-SA and 48.5-LM paths could also be due to source lightning distribution since these two paths are very similar in terms of L shell. We note that the 48.5-SU path is more active than the 48.5-SA path, which could be attributed to a combination of L shell difference and the fact that the 48.5-SA path is too far north with respect to the likely location of thunderstorm centers in the southwestern United States.

Other recent work on occurrence statistics of Trimpi events as observed in the Antarctic has shown little or no correlation with geomagnetic activity [*Leyser et al.*, 1984; *Carpenter and Inan*, 1987], although there was some tendency in earlier work for Trimpi activity to peak after magnetic storms [*Carpenter and LaBelle*, 1982]. The $\sum Kp$ for the month of October is shown in Figure 11. In comparing the $\sum Kp$ with the data in Figure 10, we find no clear association, although activity in some channels (such as NAU-SA) appears to peak either during or just after the two broad peaks in Kp (October 14 and 28). Geomagnetic activity may play a role in Trimpi event occurrence under certain conditions, but our data do not show a clear relationship.

The local time dependence of the activity for each of the paths was studied by considering the total number of events that occurred in each hour over the course of the month. Activity was generally found to be uniformly distributed over the periods of darkness on the paths, as determined by the position of the sunset/sunrise terminator at 100 km altitude.

6. Statistics of Simultaneous Events on Multiple Paths

Statistics of the events simultaneously observed on multiple paths are important in assessing the size of ionospheric disturbances, since larger regions would overlap more paths and lead to a higher likelihood of simultaneous events. Information on the sensitivity of the subionospheric VLF amplitude to disturbances located off the great circle propagation paths can also be extracted from such data since efficient scattering from distant regions would again imply a larger number of simultaneous events on the various paths shown in Figure 1.

Table 2 lists the dates/times of all the events observed during the month of October 1987 simultaneously (within 1 s) on two or more VLF paths. For each day in Table 2, the approximate UT time of the event and the paths that registered a perturbation are listed. We note that simultaneous events were mostly single isolated cases, except in the cases of October 15, 1987 (case 2), and October 27, 1987 (case 3). A few events in succession also occurred on October 21, 1987.

While Table 2 gives the general impression that simultaneous events on crossing paths are quite rare, a more quantitative assessment of such occurrences is provided in Table 3. Here, we have selected some paths as control paths and have provided the occurrence statistics from the point of view of those paths. For the 48.5-LM path, we note that only 2 (one each on October 12 and 13, 1987) out of a total of 75 events were observed simultaneously on the NAA-SU path. (Unfortunately no Saskatoon data were available for both days (Figure 10) to determine if NAU-SA and NSS-SA were perturbed.) These 75 events were distributed over 15 days and 42 hours during which events were observed on the 48.5-LM path (Figure 10), and the NAA-SU path was perturbed only in two cases (2.7%) while the NSS-SA or the NAU-SA paths were perturbed in none. Keeping in mind the assumptions discussed in section 3, this circumstance is consistent with the size of individual disturbed ionospheric regions being quite small, assuming also that the disturbed region is equally likely to be located anywhere along the 48.5-LM path. If, in fact, the event occurrence were not uniformly distributed along the 48.5-LM path and were confined to $L < 4$ (disturbances are expected to more commonly occur at lower L shells [*Carpenter and Inan*, 1987]), then the size of the regions would have to be even smaller. If all

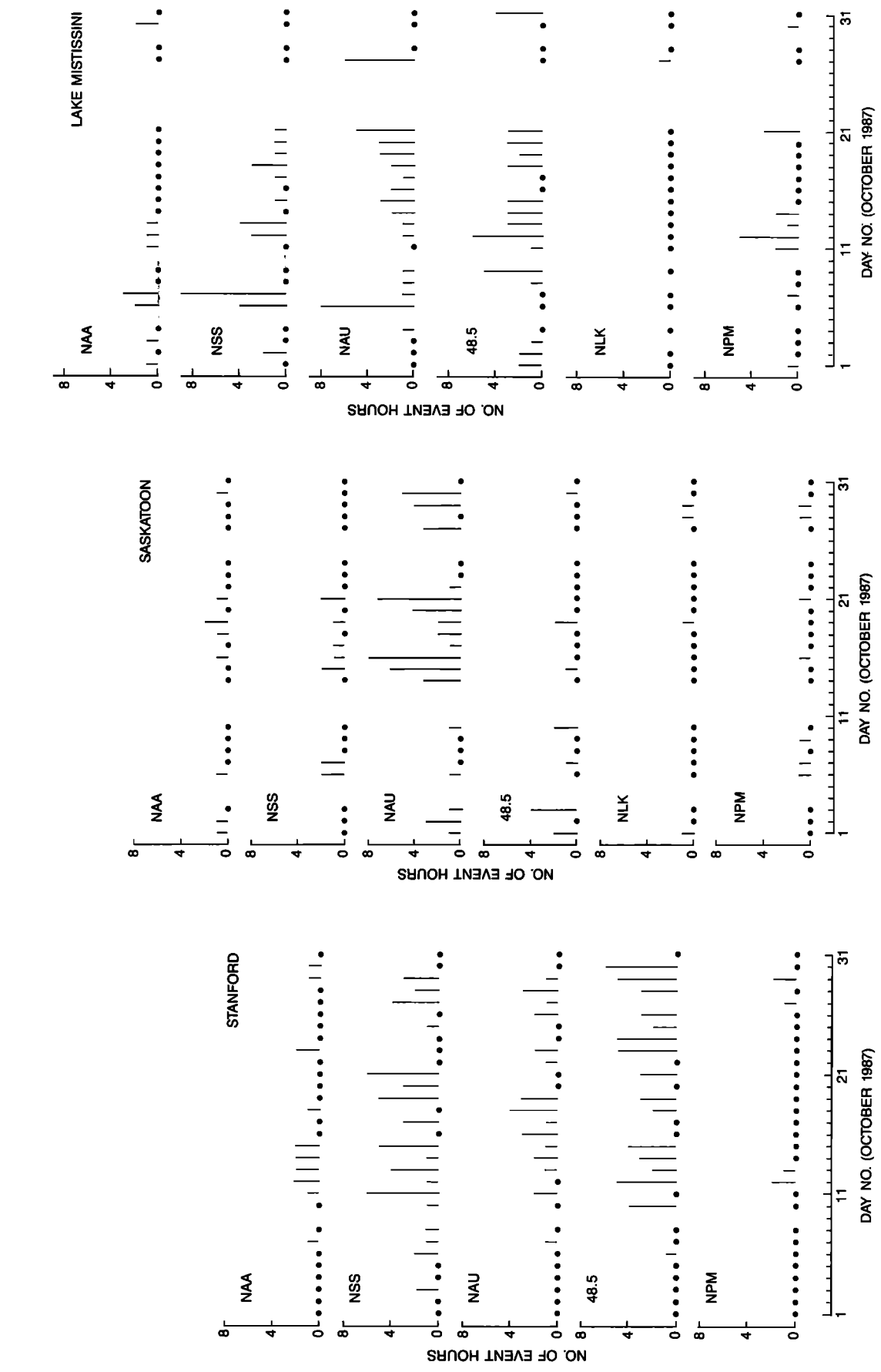

Fig. 10. Occurrence of Trimpi events for the month of October 1987 at Stanford, Saskatoon, and Lake Mistissini. For each day in October, the number of hours during which one or more VLF/LF events were detected is shown in bar graph format. Blanks indicate times when data were not available, and dots indicate that no events were observed when data were available.

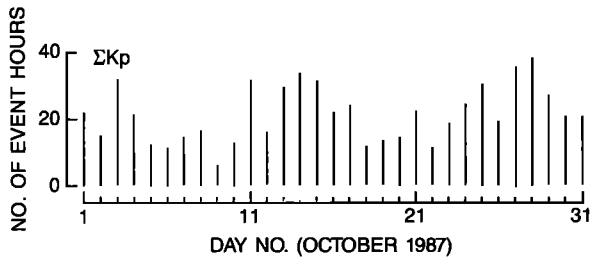

Fig. 11. The daily $\sum Kp$ for October 1987.

of the 48.5-LM events occurred closer to the transmitter end, the ionospheric regions involved would have to be < 300 km in extent, in order not to overlap the NAU-SA, 48.5-SA, and 48.5-SU paths, in addition to the region above the 48.5-kHz transmitter.

Similar observations can be made for the 48.5-SA path, which lies over a similar L shell range. Only 24 events were observed on this path, 5 of which (20.8%) were also seen on the NAA-SU path. Again assuming that disturbances are equally likely to occur anywhere along the 48.5-SA path, the fact that the NAA-SU crossing is overlapped 20% of the time is consistent with the north-south extent of disturbed regions being < 300 km. We note, however, that 3 of the 5 simultaneous events on the NAA-SU path occurred on a single day (October 15, 1987) and that the lower-latitude portions of the 48.5-SA path are more likely to be perturbed [*Carpenter and Inan*, 1987]. It thus appears that the regions involved are likely to be even smaller than 300 km in extent.

TABLE 2. Simultaneous Events Observed on Multiple Paths

Date, 1987	Time, UT	Paths Channel-Station
Oct. 1	0916	NAU-SA, NSS-SU
Oct. 3	1009	NAU-SA, NSS-SU
Oct. 10	1131:53	485-SA, NAA-SU
Oct. 12	0128	485-LM, NAA-SU
Oct. 13	0954	485-LM, NAA-SU
Oct. 14	0732	NSS-LM, NAA-SU
	0737	NAU-SA, NSS-SU
Oct. 15	0316:29	485-SA, NAA-SU 485-SU
	0318:30	NAA-SU, 485-SU NSS-SU
	0323:30	NAA-SU, 485-SU NSS-SU
	0331	NAA-SU, 485-SU NSS-SU
	0411:25	485-SA, NAA-SU 485-SU, NSS-SU
	0419	485-SU, NSS-SU
	0439:39	485-SA, NAA-SU 485-SU, NSS-SU
	0455:30	485-SU, NSS-SU
	0457	485-SU, NSS-SU
Oct. 18	0507:57	NSS-LM, NAU-LM NAA-SA, NAA-SU
Oct. 20	0652	NAU-SA, NSS-SU
	0744	NAU-SA, NSS-SU
	0814	NAU-SA, NSS-SU
Oct. 21	0625:40	NAU-SA, NSS-SU
	0631:45	NAU-SA, NSS-SU
	0634:35	NAU-SA, NSS-SU
Oct. 27	0630:30	NAU-SA, NSS-SU
	0642	NAU-SA, NSS-SU
	0657	NAU-SA, NSS-SU
	0704	NAU-SA, NSS-SU
	0705	NAU-SA, NSS-SU
Oct. 30	0813:14	485-SA, NAA-SU

TABLE 3. Occurrence Statistics of Simultaneous Events on Selected Control Paths

Control Path	Total No. of Events on Control Path	Other Path	No. of Simult. Events	% = #Simult./Total#
485-LM	75	NAA-SU	2	2.7
NSS-LM	82	NAA-SA	1	1.2
		NAA-SU	2	2.4
NAU-LM	100	NAA-SA	1	1.0
		NAA-SU	1	1.0
485-SA	24	NAA-SU	5	20.8
		485-SU	3	12.5
		NSS-SU	2	8.3
NAU-SA	91	NSS-SU	14	15.4
NAA-SA	13	NSS-LM	1	7.7
		NAU-LM	1	7.7
		NAA-SU	1	7.7
NAA-SU	22	485-LM	2	9.1
		NAU-LM	1	4.5
		NSS-LM	2	9.1
		485-SA	5	22.7
		NAA-SA	1	4.5
		485-SU	6	27.3
		NSS-SU	5	22.7
485-SU	149	485-SA	3	2.0
		NAA-SU	6	4.0
		NSS-SU	8	5.4
NSS-SU	130	NAU-SA	14	10.8
		485-SA	2	1.5
		NAA-SU	5	3.8
		485-SU	8	6.2

Another interesting control path to consider is NAU-SA. There were a total of 91 events on the NAU-SA path, 14 of which (15.4%) (distributed over 6 different days) were also registered on the NSS-SU signal. Assuming again that disturbance location along the NAU-SA path is uniformly distributed between, say, L=2 and 4, the probability of an event occurring at the crossing point would be 10-15% for 300-km-diameter circular regions. We note, however, that most events on this path may actually lie at $L < 2.5$, since the NAU-SA path shows more activity than any of the other paths at SA. On this basis, the disturbed regions are likely to be < 100 km in diameter.

Some of the control paths given in Table 3, such as 48.5-SU, are not crossed by other paths. However, noting that a total of 149 events were observed on this path and only 8 of these were simultaneous with the NSS-SU path indicates that scattering from perturbations off the great circle path is not very significant. We note that the maximum north-south separation between these two paths is ~ 100 km and that the total number of events on the 48.5-SU and NSS-SU paths is about the same. Thus, most events

occurring on the 48.5-SU and NSS-SU paths would appear to involve disturbed regions with north-south extent of < 100 km. This conclusion is also consistent with the rare occurrence of common events between the network of paths covering the northeastern region shown in Figure 1.

The path distribution as shown in Figure 1 does not allow for a more accurate estimate of the size of the disturbed regions. However, based on the above arguments and subject to the caveats discussed in section 3, it appears that the regions are generally not larger than a few hundred kilometers in extent, since this would have led to a higher occurrence of simultaneous events. It also appears that scattering by perturbations located off the great circle path is not significant, since this again would have led to a higher than observed occurrence of simultaneous events, especially in the northeastern region (Figure 1) which is covered by many adjacent paths.

That Trimpi events involve generally small (< 300 km) perturbed ionospheric regions is consistent with the precipitation of electrons being caused primarily by ducted whistlers. The circumstances of case 2, involving two distinctly different disturbed regions, are also consistent with this and would be understood as two different magnetospheric ducts being excited by the same lightning flash. However, past work has uncovered some evidence that nonducted whistlers may also cause lightning-induced electron precipitation events [*Voss et al.*, 1984; *Inan et al.*, 1988*a*] and it is difficult to determine the relative roles of ducted versus nonducted whistlers from our data alone. We note that perturbed ionospheric regions may still be expected to be relatively small in nonducted events, since the most intense whistler waves would be injected immediately above the thunderstorm regions. Association of events with ducted whistlers can be made using broadband VLF data on ducted whistlers observed in regions conjugate to the source lightning activity [*Inan and Carpenter*, 1987]. For the October 1987 period studied here, such data were only available on a discontinuous basis and for synoptic periods (1 min out of every 15) from Lake Mistissini. Examination of these data for the few periods studied did not provide any new information since no whistlers or other VLF activity were observed.

7. Summary

We have shown that observations of signals propagating over distributed sets of subionospheric VLF paths can provide a data base with which we can estimate the spatial distribution and occurrence of lightning-induced electron precipitation effects. Event activity over continent size regions can be studied, and simultaneous observations of individual events on subionospheric paths that "cross" one another allow localization of the disturbed ionospheric region(s) subject to the assumptions and caveats discussed in section 3. Absence of perturbations on nearby paths can provide an assessment of the spatial extent of the region with a varying degree of accuracy, depending on the distribution of signal paths under study and the modal structure of the propagation along each path. In case 2, we observed distinctly different onset delays with respect to the causative spheric in simultaneous events on two different paths, with an L dependence consistent with predictions of whistler-particle scattering theory. This type of behavior was interpreted as strong evidence of two distinct regions separated in L shell by $\sim 0.4L$ excited in individual events. Occurrence statistics over the course of October 1987 are consistent with generally higher levels of activity at the lower-latitude end of the $2 < L < 4$ range, although it is difficult to separately assess the role of the source lightning distribution. Occurrence statistics of simultaneous events on crossing paths are consistent with the spatial extent of the disturbed ionospheric regions being less than a few hundred kilometers. The relatively low occurrence of simultaneous events on adjacent paths also suggests that scattering from disturbances located off (by >100 km) the great circle paths is not likely to be significant.

Acknowledgments. We thank our colleagues in the VLF group for many useful discussions and especially W. Burgess for his comments on the paper. We are grateful to D. McEwen and colleagues at the University of Saskatchewan for facilitating the placement and operation of the Stanford VLF system at Saskatoon. The manuscript was prepared by Zheng Xu. The VLF data at Stanford were acquired during system and engineering testing of equipment destined for Palmer station in the context of the research work under National Science Foundation grant NSF-DPP-86-11623. This research was supported by the National Science Foundation under grant ATM-88-04273.

The Editor thanks R. H. Holzworth and J. LaBelle for their assistance in evaluating this paper.

References

Carpenter, D. L., and U. S. Inan, Seasonal, latitudinal and diurnal distributions of whistler-induced electron precipitation events, *J. Geophys. Res.*, *92*, 3492, 1987.

Carpenter, D. L., and J. W. LaBelle, A study of whistlers correlated with bursts of electron precipitation near $L = 2$, *J. Geophys. Res.*, *87*, 4427, 1982.

Carpenter, D. L., and N. T. Seely, Cross-L plasma drifts in the outer plasmasphere: Quiet time patterns and some substorm effects, *J. Geophys. Res.*, *81*, 2728, 1976.

Chang, H. C., and U. S. Inan, Lightning-induced electron precipitation from the magnetosphere, *J. Geophys. Res.*, *90*, 1531, 1985.

Dowden, R. L., and C. D. D. Adams, Phase and amplitude perturbations on subionospheric signals explained in terms of echoes from lightning-induced electron precipitation ionization patches, *J. Geophys. Res.*, *93*, 11543, 1988.

Dowden, R. L., and C. D. D. Adams, Phase and amplitude perturbations on the NWC signal at Dunedin from lightning-induced electron precipitation, *J. Geophys. Res.*, *94*, 497, 1989.

Goldberg, R. J., J. R. Barcus, L. C. Hale, and S. A. Curtis, Direct observation of magnetospheric electron precipitation stimulated by lightning, *J. Atmos. Terr. Phys.*, *48*, 293, 1986.

Inan, U. S., and D. L. Carpenter, On the correlation of whistlers and associated subionospheric VLF/LF perturbations, *J. Geophys. Res.*, *91*, 3106, 1986.

Inan, U. S., and D. L. Carpenter, Lightning-induced electron precipitation events observed at $L = 2.4$ as phase and amplitude perturbations on subionospheric VLF signals, *J. Geophys. Res.*, *92*, 3293, 1987.

Inan, U. S., D. L. Carpenter, R. A. Helliwell, and J. P. Katsufrakis, Subionospheric VLF/LF phase perturbations produced by lightning-whistler induced particle precipitation, *J. Geophys. Res.*, *90*, 7457, 1985.

Inan, U. S., W. C. Burgess, T. G. Wolf, D. C. Shafer, and R. E. Orville, Lightning-associated precipitation of MeV electrons from the inner radiation belt, *Geophys. Res. Lett.*, *15*, 172, 1988*a*.

Inan, U. S., D. C. Shafer, W. Y. Yip, and R. E. Orville, Subionospheric VLF signatures of nighttime D region perturbations in the vicinity of lightning discharges, *J. Geophys. Res.*, *93*, 11455, 1988*b*.

Inan, U. S., T. G. Wolf, and D. L. Carpenter, Geographic distribution of lightning-induced electron precipitation observed as VLF/LF perturbation events, *J. Geophys. Res.*, *93*, 9841, 1988*c*.

Leyser, T. B., U. S. Inan, D. L. Carpenter, and M. L. Trimpi, Diurnal variation of burst precipitation effects on subionospheric VLF/LF signal propagation near $L = 2$, *J. Geophys. Res.*, *89*, 9139, 1984.

Lohrey, B., and A. B. Kaiser, Whistler-induced anomalies in VLF propagation, *J. Geophys. Res.*, *84*, 5122, 1979.

Park, C. G., D. L. Carpenter, and D. B. Wiggin, Electron density in the plasmasphere: Whistler data on solar cycle, annual, and diurnal variations, *J. Geophys. Res.*, *83* (A7), 3137, 1978.

Poulsen, W. L., T. F. Bell, and U. S. Inan, Three-dimensional modeling of subionospheric VLF propagation in the presence of localized D region perturbations associated with lightning, *J. Geophys. Res.*, *95*, 2355, 1990.

Rycroft, M. J., Enhanced energetic electron intensities at 100 km altitude and a whistler propagating through the plasmapause, *Planet. Space Sci.*, *21*, 239, 1973.

Tolstoy, A., T. J. Rosenberg, and D. L. Carpenter, The influence of localized precipitation-induced *D* region ionization enhancements on subionospheric VLF propagation, *Geophys. Res. Lett.*, *9*, 563, 1982.

Tolstoy, A., T. J. Rosenberg, U. S. Inan, and D. L. Carpenter, Model predictions of subionospheric VLF signal perturbations resulting from localized, electron precipitation-induced ionization enhancement regions, *J. Geophys. Res.*, *91*, 13473, 1986.

Voss, H. D., W. L. Imhof, M. Walt, J. Mobilia, E. E. Gaines, J. B. Reagan, U. S. Inan, R. A. Helliwell, D. L. Carpenter, J. P. Katsufrakis, and H. C. Chang, Lightning-induced electron precipitation, *Nature*, *312*, 740, 1984.

Wolf, T. G., Remote sensing of ionospheric effects associated with lightning using very low frequency radio signals, Ph.D. thesis, Stanford Univ., Stanford, Calif., 1990.

U. S. Inan, F. A. Knifsend, and J. Oh, STAR Laboratory, Department of Electrical Engineering/SEL, Stanford University, Stanford, CA 94305.

(Received February 26, 1990;
revised April 26, 1990;
accepted May 22, 1990.)